An Algorithm for the Detection of Fronts in Wind Profiler Data

CHRISTOPHER LUCAS

Department of Physics and Mathematical Physics, University of Adelaide, Adelaide, Australia

PETER T. MAY

Bureau of Meteorology Research Centre, Melbourne, Australia

ROBERT A. VINCENT

Department of Physics and Mathematical Physics, University of Adelaide, Adelaide, Australia

(Manuscript received 23 December 1999, in final form 10 August 2000)

ABSTRACT

An algorithm to detect frontal zones in time–height cross sections of horizontal wind from wind profiler measurements is described. The algorithm works by identifying regions with 1) a strong horizontal temperature gradient, estimated by using a quasigeostrophic thermal wind retrieval, 2) a strong temporal increase in the signal-to-noise ratio at a given range gate, and/or 3) a strong temporal shift in the horizontal winds at a given range gate. The type (e.g., cold or warm) of front is determined by examining the advection field and the characteristics of the boundary. Most weight is given to the horizontal temperature gradient component of the algorithm.

A springtime frontal system and an associated baroclinic wave over South Australia are examined using both routine synoptic observations and analyses as well as data from the profiler. Synoptic observations depict a prefrontal trough and two cold fronts at the surface and a deep trough in upper levels. The tropopause is identified at ~6 km in one sounding. The algorithm successfully identifies the one main cold front and the lowered tropopause in the polar air. There are also hints of a prefrontal trough and a descending tropopause with the onset of the main cold front. After the passage of the upper trough, the ascending tropopause and the so-called jet front or trailing front are also identified by the algorithm. The latter represents the passage of the upper-level baroclinic wave and the reappearance of a strong jet stream.

Other regions are spuriously identified as fronts. These regions could be the reflection of some short-term meteorological phenomena, such as gravity waves; deviations from the assumed quasi-geostrophy; or simply reflections of noise in the analysis. An examination of the effect of random measurement uncertainties on the frontal analysis gives an estimate of error of around 2 K $(100\ \text{km})^{-1}$ in the horizontal temperature gradient calculations for typical wind errors. The errors on the retrieved advection vary, depending on the wind speed, but are around 25 K day^{-1} for a ~20 m s^{-1} wind speed. These values are typical of the noise in those fields, suggesting that the spuriously defined fronts likely reflect uncertainties in the data rather than actual meteorological phenomena.

1. Introduction

Fronts and frontal systems are important midlatitude weather features and are responsible for much of the clouds and precipitation observed in those regions. Traditionally, the structure and dynamics of frontal systems in the troposphere have been examined using rawinsonde networks with synoptic-scale spacing (~400 km) and 12-h time resolution (see Shapiro and Keyser 1990 for a review). Since the 1970s, radar wind profilers have provided high-quality observations of the horizontal and vertical wind with a temporal resolution of an hour or less. This technology has allowed the features of frontal systems to be readily observed in unprecedented detail (Shapiro et al. 1985; Neiman et al. 1992).

Previous investigators have used a variety of methods to identify fronts and their characteristics using data from radar wind profilers. Larsen and Röttger (1985) identified upper-level frontal zones in five cases by noting the increase in reflectivity associated with the enhanced stability of the frontal zone. Echo power enhancement at frontal boundaries is seen most reliably in the upper levels (e.g., Larsen and Röttger 1982, 1983; May et al. 1991). This is because in the upper tropo-

Corresponding author address: Dr. Christopher Lucas, Department of Physics and Mathematical Physics, University of Adelaide, Adelaide 5005, Australia.
E-mail: clucas@physics.adelaide.edu.au

© 2001 American Meteorological Society

Unauthenticated | Downloaded 10/19/21 07:43 PM UTC

sphere the static stability terms of the refractive index gradient dominate, while below about 500 hPa the moisture terms are greater (Tsuda et al. 1988). Frontal gradients are sometimes seen in regions where the moist terms dominate, but in general the large spatial variability in humidity masks these boundaries.

Neiman and Shapiro (1989) described a methodology for calculating the horizontal temperature gradient and thermal advection associated with fronts using data from a single profiler. They found that the timing, altitude, and magnitude of the profiler-derived quantities agreed with those observed by the operational rawinsonde network. They also discussed the limitations to this approach in the presence of ageostrophy, curvature in the flow, and when the ageostrophy and curvature vary with height. Crochet et al. (1990) examined the mesoscale characteristics of several fronts near the coast of France using a very high frequency (VHF) Doppler radar. In that study, fronts were subjectively analyzed using surface charts and instruments located near the profiler. May et al. (1990) and Griffiths et al. (1998) used profiler data to focus on observations of fronts and their associated mesoscale circulations in southern Australia. Neiman et al. (1992) showed that the characteristics of fronts derived from qualitatively combining wind profilers and Radio Acoustic Sounding Systems compared favorably with the results obtained from more traditional observing systems and allowed for mesoscale features of frontal systems to be resolved on hourly timescales. Browning et al. (1998) combined data from UHF and VHF wind profilers to identify mesoscale characteristics of a cold frontal system in Wales, including the upper-level and low-level jets, the rearward sloping warm-conveyor belt flow, a rear-inflow, and an associated tropopause fold. Caccia and Cammas (1998) used the ratio of vertical-to-oblique echo power to describe the tropopause break, slope, and turbulence characteristics of an upper-level frontal zone. In all of these studies, the locations of the fronts in question were subjectively determined.

The goal of this paper is to describe an algorithm to identify frontal zones in time–height cross sections of horizontal wind from radar wind profiler data. The algorithm objectively identifies regions that are potentially frontal zones, but the interpretation of the results is subjective. Data from other sources are not used in the scheme. Such an algorithm allows for a quick and consistent identification of frontal zones that pass over the profiler site. Our intent is to use this algorithm in a future paper to construct a census of frontal systems in South Australia and document their physical characteristics throughout the year. The algorithm could also be run in real time in order to aid in the diagnosis and forecasting of frontal systems. Additionally, the scheme can be easily adapted for use with output from operational forecast models for verification studies.

Section 2 briefly describes the characteristics of the wind profiler and the source of the analyzed weather data. Section 3 details the workings of the front-finding algorithm. Section 4 presents a case study of a strong springtime frontal system from the point of view of a traditional synoptic analysis and the radar wind profiler. The results of the front-finding algorithm are demonstrated. With the provided example in mind, possible sources of error and limitations of the algorithm are discussed in section 5. Section 6 provides a summary and basic conclusions of this study.

2. Data

The data used in the study come from the VHF wind profiler located at Mount Gambier (37.7°S, 140.7°E) in southeastern South Australia, a location near the coast[1] (Reid et al. 1998). This profiler operates at 44.7 MHz and has been in nearly continuous operation since January 1998. During the time of this study, horizontal and vertical winds in the troposphere were sampled approximately every 1 min using the spaced-antenna method (Briggs 1984) from a single vertically pointing beam. These data are averaged to give a temporal resolution of 1 h. Data extend from 1.5 km to a nominal height of 15 km with a vertical resolution of 300 m. Winds are reliably available up to 8 km, although this range can extend upward depending on the meteorological circumstances.

The profiler data are supplemented with routine observations and analyses from the Australian Bureau of Meteorology (BoM). Upper-air data are derived from radiosonde and wind flights at Mount Gambier. Upper winds are generally reported four times daily. The thermodynamic structure is reported once per day at 0000 UTC, with an occasional supplemental sounding at 1200 UTC. Analyses at the surface and 500 hPa are taken from the BoM Limited Area Prediction System (LAPS) operational forecast model (Puri et al. 1998). At the time of the case study, the model used a horizontal resolution of 0.75°. Recently, the horizontal resolution has been increased to 0.375°. Frontal positions are taken from the operational manual surface analysis.

3. Description of the algorithm

Both surface and upper-level fronts are characterized by large horizontal temperature gradients, static stability, absolute vorticity, and vertical wind shear (Keyser and Shapiro 1986). At a single observation point, the large absolute vorticity is manifest as a change in the direction and speed of the horizontal wind in the cross-front direction. In this study, these definitions and the techniques used by previous investigators to identify frontal boundaries in profiler data are utilized to create the algorithm described herein. It is sought to create an

[1] Local time = UTC + 9.5 h.

Unauthenticated | Downloaded 10/19/21 07:43 PM UTC

TABLE 1. Description of scoring for the front-finding algorithm.

Quantity	Scores
Gradient strength	1 point for 1.5–3.0 K (100 km)$^{-1}$ 1 point for each additional 0.5 K (100 km)$^{-1}$
SNR increase	0.5 points for 2.5–3.0 dB 0.5 points for each additional 1.5 dB
Temporal vector wind change	1.0 point for 5.0–7.5 m s^{-1} change 0.5 points for each additional 2.5 m s^{-1} Half points given if not associated with gradient $\geq$ 1.5 K (100 km)$^{-1}$ or SNR change $\geq$ +2.5 dB

algorithm sensitive enough to identify weak frontal boundaries, but not so sensitive as to produce a large number of false alarms. However, some noise is inevitable and a subjective judgement is ultimately required.

The algorithm works by identifying regions that contain 1) a strong horizontal thermal gradient, as identified using the method described by Neiman and Shapiro (1989); 2) a strong wind shift in time at a given range gate; and/or 3) a sharp temporal increase in the signal-to-noise ratio (SNR), which is proportional to the radar reflectivity, at a given range gate. The wind shift and SNR differences are computed from the ''prevailing values,'' averages 3 h prior to the time at which the score is being computed. A score is assigned to each valid data point in the time–height domain based on the strength of quantities listed above.

The criteria and methods for assigning the scores are shown in Table 1. The values are somewhat arbitrary and derived from an empirical examination of the data shown here and from other cases. To arrive at these criteria, the main cold fronts in selected cases were first identified subjectively. The variables were then tuned to achieve the best match with the subjective front while minimizing spuriously defined frontal boundaries.

The primary criterion for determining the frontal scores is the retrieved gradient calculation. As mentioned above, a defining characteristic of fronts is a large horizontal temperature gradient and the calculation is reasonably robust where the wind is in approximate geostrophic balance. The correspondence of gradients retrieved in this manner with a frontal zone in a quasi-balanced flow regime was demonstrated by Neiman and Shapiro (1989). In addition, they described how non-balanced flow regimes associated with gravity waves reduce the reliability of the technique, leading to the identification of nonfrontal horizontal gradients.

The SNR criterion is included primarily to capture the upper-level (say, >8 km) portions of the frontal zone, where there are often insufficient wind data to compute the gradient. As shown by Larsen and Röttger (1985), May et al. (1991), and others, this increase in returned power is a reliable method of detecting fronts at these altitudes. However, SNR is often a noisy field, with variability related to subtle changes in the refractivity above the profiler that are often unconnected with frontal zones. To reduce this noise, frontal scores are calculated from prevailing values and a lower relative weight is given to this portion of the algorithm.

The scores from the temporal wind change criterion are computed based on the magnitude of the vector difference in the wind at the time of interest and the prevailing value. Again, the prevailing value is used in order to reduce noise in the computation. Using the vector wind change allows for changes in direction to be included. If the wind change corresponds with a horizontal gradient or SNR jump of sufficient magnitude to score points, full points are given. Otherwise, the wind change score is reduced by half. This methodology emphasizes wind changes associated with likely frontal zones while discounting wind changes due to error or other, nonfrontal meteorological phenomena.

Once computed, the scores are contoured and regions enclosed by the contours that display continuity with time and height are identified as fronts. By examining the advection pattern, calculated from the retrieved horizontal temperature gradient and profiler winds (Neiman and Shapiro 1989), and the physical characteristics of the boundary, the front can be identified as a cold, warm, or upper-level front. Further classification can be made as necessary. These are manual, subjective processes. Fronts can be reliably detected as low as the second available profiler range gate. This is the first point for which the retrieved thermal gradient and advection are computed.

4. An example

As a demonstration of the front-finding algorithm, a well-defined surface and upper-level frontal passage over South Australia from 17 to 19 October 1998 is examined. First, the synoptic setting is described from analyses of the BoM. The synoptic discussion is followed by a discussion of the profiler data from Mount Gambier.

a. Synoptic overview

Charts and graphs derived from standard observations for the period of interest are presented in Figs. 1–4. Figure 1 shows measurements of temperature, dewpoint, pressure, and wind at the surface from Mount Gambier for the period 16–20 October. The time resolution of these observations is 30 min and winds are plotted every 3 h

Unauthenticated | Downloaded 10/19/21 07:43 PM UTC

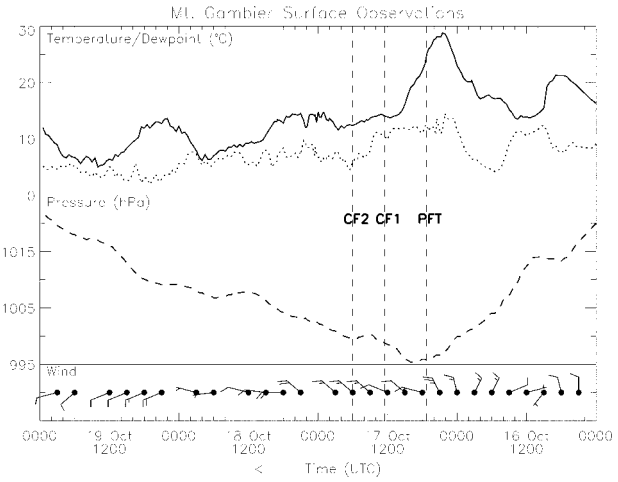

FIG. 1. Time series of surface observations from Mount Gambier. Shown are temperature (solid, °C; top) and dewpoint (dots, °C; top), pressure (dashed, hPa; middle), and wind (barbs; bottom). Temporal resolution of observations is 30 min. Wind barbs plotted every 3 h for clarity. Wind barbs: pennant = 25 m s^{-1}; long barb = 5 m s^{-1}; short barb = 2.5 m s^{-1}.

for clarity. The daily surface analyses (Fig. 2) are from 1100 UTC each day and are a compilation of the numerical analyses from the Australian operational LAPS model and the manual operational analyses. Frontal positions are taken directly from the operational analyses. Fronts and cyclones analyzed over the ocean are based largely on interpretation of satellite data; no other data are available to refine and/or verify the analyses. The daily 500-hPa charts (Fig. 3) are also taken from the LAPS analysis at 1100 UTC. The patterns depicted in those charts are also representative of the large-scale flow at greater heights (e.g., 250 hPa), where the troughs and jet streaks are located in approximately the same position. Finally, the available upper-air thermodynamic soundings and corresponding winds are shown in Fig. 4.

The surface observations 1 day prior to the period of interest, 16 October, show pressure decreasing from 1020 to 1000 hPa by the end of the day. Winds are generally northerly, with a weak sea breeze in the late afternoon, as evidenced by the SW surface flow at 0900 UTC. A modest diurnal cycle is apparent in the temperature data.

On 17 October, the surface analysis (Fig. 2a) depicts a complex system of cyclones and fronts approaching South Australia (SA). Shown are two fronts (denoted CF1 and CF2) and a prefrontal trough (PFT). The parent cyclone of PFT and CF1 is located in the Southern Ocean, well off the map at 55°S, 150°E, while CF2 is associated with a smaller closed low, partially visible in Fig. 2, at 45°S, 140°E. The 500-hPa analysis at 1100 UTC on 17 October (Fig. 3a) shows a broad trough with a WNW jet streak with speeds in excess of 50 m s^{-1} extending from Western Australia (WA) to Tasmania. The radiosonde launched at 2302 UTC 16 October, just prior to the time of interest (Fig. 4a), shows wind speeds of ~80 m s^{-1} around the 200-hPa level. Temperatures

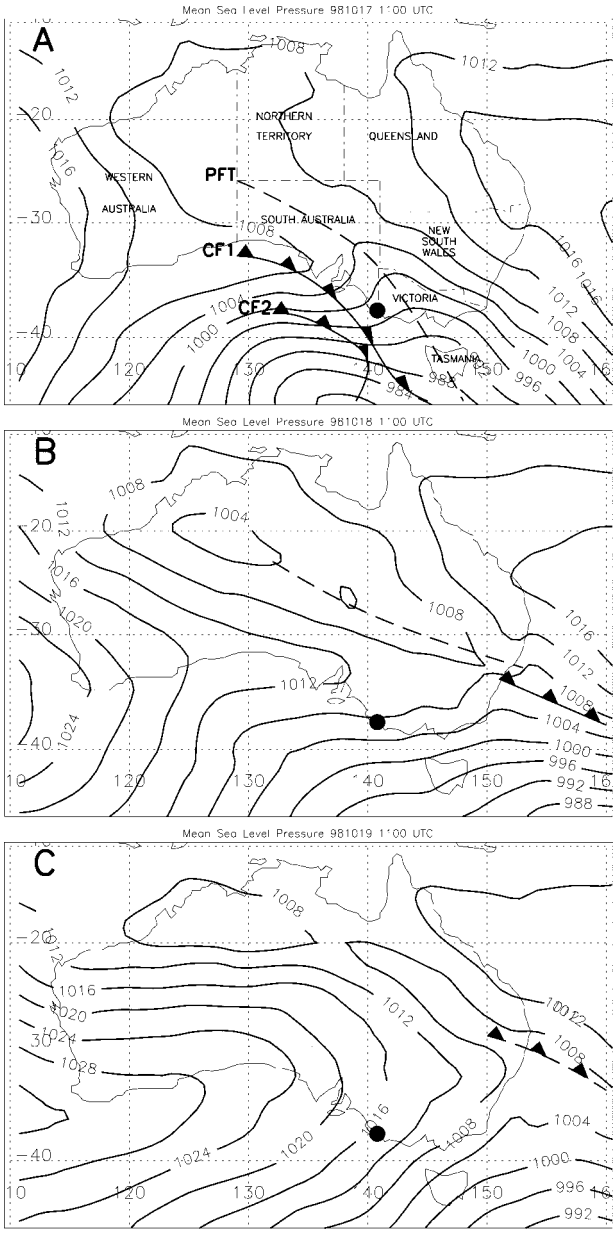

FIG. 2. Sea level pressure (hPa) from LAPS and operational frontal analyses at 1100 UTC on (a) 17 Oct, (b) 18 Oct, and (c) 19 Oct 1998. Australian state names and boundaries shown in (a). Location of Mount Gambier, South Australia, denoted by large dot. Contour interval is 4 hPa.

in the lower troposphere are quite warm, exceeding 25°C in the inversion near 1 km. The tropopause, using the lapse rate–based definition of the World Meteorological Organization (WMO 1957),[2] is at 13.2 km.

During the course of the day, PFT, CF1, and CF2 all

[2] The WMO defines the tropopause as the first point on a sounding above which the lapse rate is ≤2°C km^{-1} for at least 2 km.

Unauthenticated | Downloaded 10/19/21 07:43 PM UTC

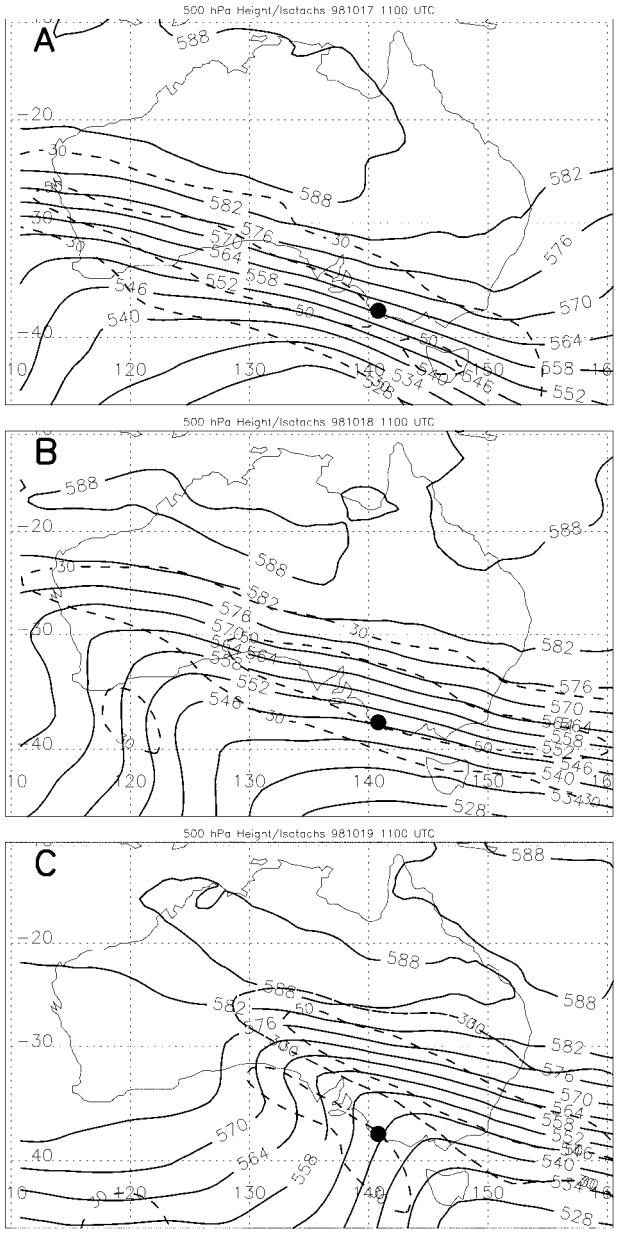

FIG. 3. LAPS 500-hPa heights (dam; solid) and isotachs (m s^{-1}, dashed) at 1100 UTC on (a) 17 Oct, (b) 18 Oct, and (c) 19 Oct 1998. Contour intervals are 6 dam and 20 m s^{-1} beginning at 30 m s^{-1}.

cross Mount Gambier and move inland. Approximate times of passage of each of these features are noted in Fig. 1 as dashed vertical lines. Before the passage of PFT, surface temperatures are quite warm, exceeding 29°C, and northerly winds exceeding 12.5 m s^{-1} are observed. With the passage of PFT around 0500 UTC, pressure nears its minimum value of 995 hPa, temperature decreases rapidly, and the wind shifts to a more westerly direction and slows. By comparison, the nocturnal passages of CF1 (~1230 UTC) and CF2 (~1800 UTC) have relatively little effect on the winds and temperature. No precipitation was reported on this day. Both fronts dissipate quickly after moving ashore. Hanstrum et al. (1990) have noted similar interactions between the PFT and cold fronts over southern Australia previously, with the PFT often developing at the expense of the preexisting surface cold fronts. In addition to the surface changes, a strong temperature drop is also noted during the day in the lowest 3 km of the troposphere in the sounding data (Figs. 4a,b). The tropopause descends to 12.0 km, but the strong jet remains centered at ~250 hPa.

On 18 October, the surface cyclone of PFT and CF1 has migrated to the southeast, while the surface cyclone of CF2 has dissipated. The remnants of PFT, CF1, and CF2 have been merged in the analysis (and denoted as a trough) and pushed well inland over central and eastern Australia (Fig. 2b). High pressure builds over SA and the maximum surface temperature at Mount Gambier is ~14°C cooler than the previous day (Fig. 1). The surface wind turns to a more westerly direction and gradually weakens during the day. A total of 3 mm of rain was reported on this day. The broad trough at 500 hPa sharpens, with the main axis extending from 50°S, 140°E (off the map) to southern WA (Fig. 3b). A WNW jet streak with winds in excess of 50 m s^{-1} remains over SA. With the exception of the layer of drier air centered at ~2.5 km, the sounding for this day at 2300 UTC (Fig. 4c) shows relatively cool and moist conditions below 5.5 km. Above that altitude, the air is very dry with a weak lapse rate (~2°–3°C km^{-1}), suggestive of a downward intrusion of stratospheric air and a lowered tropopause, although the lapse rate is just above that required to meet the official definition given by the WMO. Zonal cross sections of potential vorticity (PV, not shown) from the LAPS model depict PV values characteristic of stratospheric air as low as 500 hPa over Mount Gambier at the time of the sounding in Fig. 4c, further suggesting a tropopause fold at that time.

On 19 October, the remnants of the surface front, now only apparent as a trough, have pushed well north into Queensland. A broad ridge extends across the southern portion of the continent (Fig. 2c) and pressure has increased to over 1020 hPa. Surface wind has turned to the SW and temperatures at the surface are relatively cool. Total rainfall of 2 mm was reported during the day. The sharp trough at 500 hPa has moved eastward over Tasmania and SA. The axis of this trough is over Mount Gambier at this time. Behind the trough, southerlies in excess of 30 m s^{-1} are indicated. The jet streak has moved inland, with speeds exceeding 50 m s^{-1} over a broad area (Fig. 3c). The sounding at 2300 UTC for this day (Fig. 4d) shows a sharp inversion at ~1.5 km. Just above this inversion, the wind turns sharply to the SSW and increases in speed by 5 m s^{-1}. The tropopause is located around 10.7 km. A comparatively weak jet of 35 m s^{-1} is found around that level.

b. Profiler data

Figure 5 shows a time–height cross section of horizontal wind from the VHF profiler from 0000 UTC 17

Unauthenticated | Downloaded 10/19/21 07:43 PM UTC

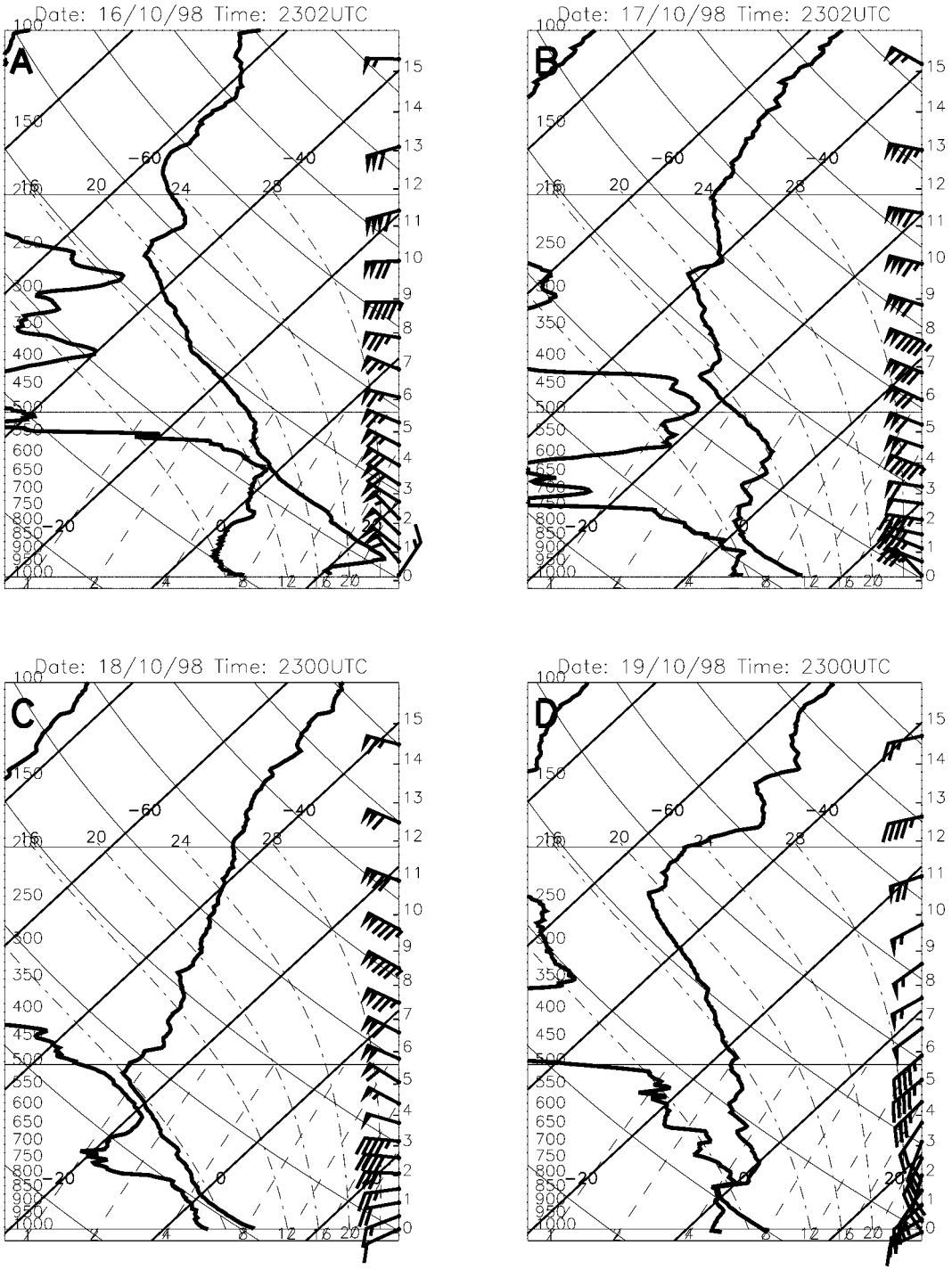

FIG. 4. Temperature, dewpoint, and winds from radiosonde flights at Mount Gambier in skew *T*–log*p* format at 2300 UTC for (a) 16 Oct, (b) 17 Oct, (c) 18 Oct, and (d) 19 Oct 1998. Wind barbs as in Fig. 1. Climatological heights also shown.

October to 1200 UTC 18 October. Height ranges from 1 to 12 km and reflects the height above ground level (69 m above sea level at Mount Gambier). Time runs from right to left in this and the following diagrams. Wind barbs are plotted every 2 h for clarity. Isotachs are also shown for speeds above 30 m s^{-1}. The flow is largely dominated by NW to WNW winds. Wind speeds generally increase throughout the first half of the period, remaining relatively constant in the latter half. Wind speeds also increase with height. Speeds at 5.5 km

Unauthenticated | Downloaded 10/19/21 07:43 PM UTC

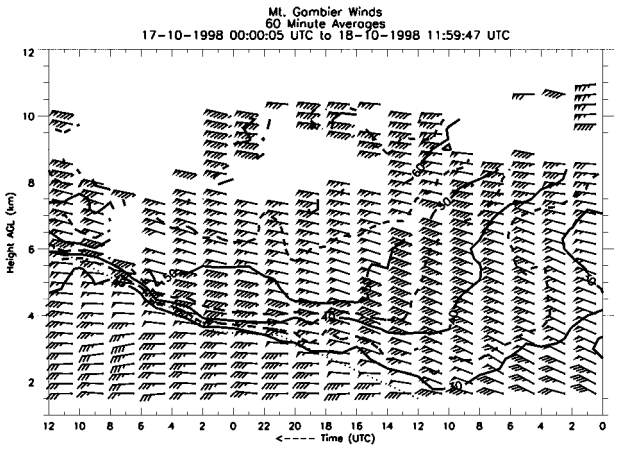

FIG. 5. Time–height cross section of hourly averaged horizontal wind from the Mount Gambier VHF wind profiler from 0000 UTC 17 Oct to 1200 UTC 18 Oct 1998. Winds plotted every 2 h for clarity. Time runs from right to left. Wind barbs as in Fig. 4. Isotachs (contours) with 5 m s^{-1} interval beginning at 30 m s^{-1} also shown. Dotted line represents the wind shift line mentioned in text. Vertical axis is height above ground level (69 m at Mount Gambier).

(~500 hPa) range from 30 m s^{-1} at 0000 UTC to 55 m s^{-1} at 2200 UTC, in good agreement with the 500-hPa synoptic charts at 1100 UTC on 17 and 18 October (Figs. 3a and 3b). These strong WNW winds continue into 18 October above 6-km altitude. Beginning at the lowest heights (~1.5 km) around 1200 UTC on 17 October, a change in the wind direction and speed at a given range gate can be observed (denoted by dotted line). This wind shift moves upward in time, reaching 6 km by 1200 UTC on 18 October. After the shift, winds weaken and turn to a more westerly direction. This weakening is readily apparent as a ''convergence'' of the isotachs. Coincident with this temporal change in horizontal wind, a strong horizontal temperature gradient is indicated (Fig. 6). The magnitude of this gradient exceeds 7 K (100 km)$^{-1}$ in several places. Early on 17 October, a gradient that descends in time from ~3.5 km to the lowest levels is apparent.

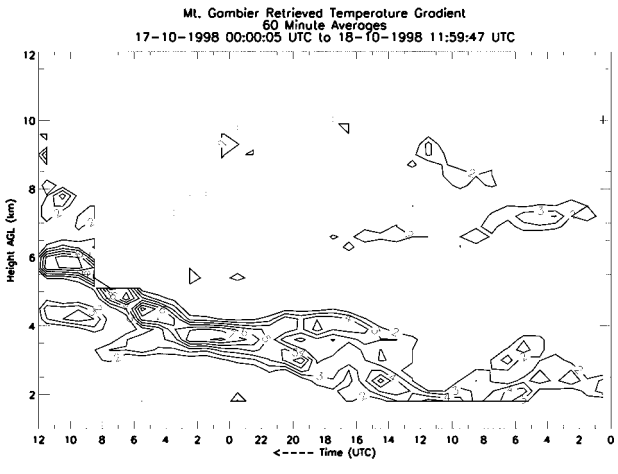

FIG. 6. As in Fig. 5 except for retrieved horizontal temperature gradient [K (100 km)$^{-1}$]. Contour interval is 1 K (100 km)$^{-1}$ beginning at 2.

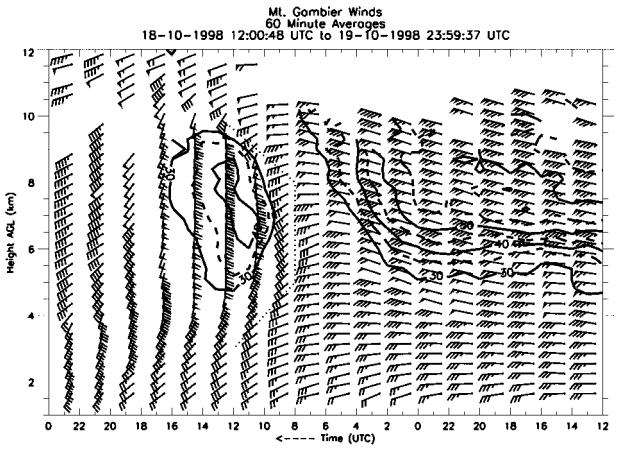

FIG. 7. As in Fig. 5 except for 1200 UTC 18 Oct to 0000 UTC 20 Oct 1998.

Figure 7 shows a time–height cross section of horizontal wind from 1200 UTC 18 October to 0000 UTC 20 October. On the latter half of 18 October, the flow below 6 km remains generally westerly. Above 6 km, the strong jet streak is indicated, with wind being generally WNW with speeds from 50 to 80 m s^{-1}. The wind shift line from the previous period (Fig. 5) is not seen in the latter half of 18 October. Around 1000 UTC on 19 October, the flow changes abruptly. Strong S and SW winds with speeds around 30–40 m s^{-1} begin at 6-km altitude. This wind shift line (denoted as a dotted line) moves both upward and downward with time, moving down to near 2 km and up to 10+ km. Retrieved horizontal temperature gradients for this time period are shown in Fig. 8. The gradient that rose from 2 to 6 km during the previous period remains between 6 and 7 km until 0600 UTC on 19 October. The gradient is strong

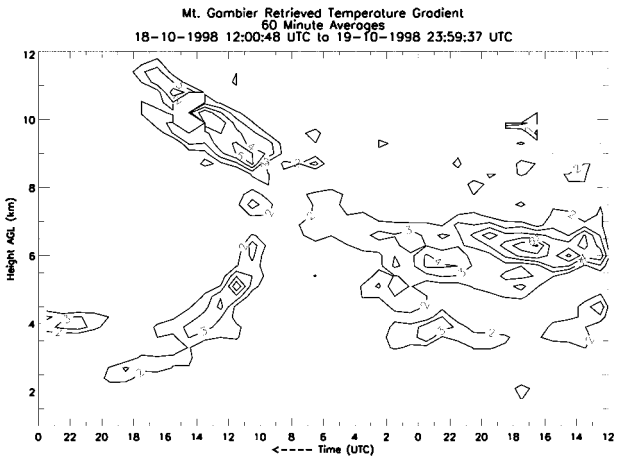

FIG. 8. As in Fig. 6 except for 1200 UTC 18 Oct to 0000 UTC 20 Oct 1998.

Unauthenticated | Downloaded 10/19/21 07:43 PM UTC

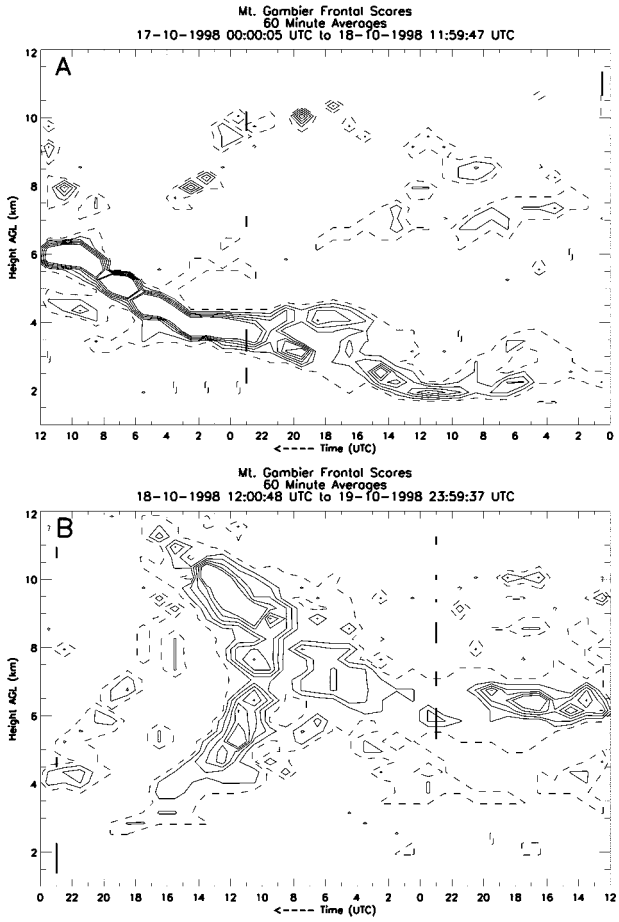

FIG. 9. As in Fig. 5 except for frontal scores as determined by the algorithm for (a) 0000 UTC 17 Oct to 1200 UTC 18 Oct 1998 and (b) 1200 UTC 18 Oct to 0000 UTC 20 Oct 1998. Contour interval is 1. Dashed line represents a score of 1. Vertical bars represent regions with a lapse rate of less than 3°C km^{-1} from the sounding data.

initially, with peaks of 6 K (100 km)$^{-1}$, but fades during 18 October. Coincident with the onset of the S and SW winds, strong gradients are again seen, with peaks exceeding 5 K (100 km)$^{-1}$.

Figure 9a shows contours of the frontal scores as calculated using the algorithm described above for 0000 UTC 17 October to 1200 UTC 18 October. The contour interval is 1 and the dashed contour indicates a score of 1. Only one frontal feature is readily identifiable at these heights. This one main front can be readily identified, extending upward from 2 km at 1100 UTC on 17 October to 6 km at 1200 UTC on 18 October. This front is associated with the strong gradient and temporal wind shift previously discussed (Figs. 5, 6). The frontal positions detected by the profiler can by verified by examining the sounding data shown in Fig. 4. In radiosonde data, a frontal boundary appears as a region of enhanced thermal stability, as warm air overrides the cold air. Obviously, not every layer with a low lapse rate identified in the sounding data is associated with a frontal zone. Stable layers can and do appear in these data independently of frontal zones. The location of regions with a lapse rate of <3°C km^{-1} in the sounding data is denoted by vertical bars in Fig. 9. The two analyses agree reasonably well. The frontal positions in the profiler data generally have an associated stable layer in the sounding data. Stable layers other than those associated with the main profiler-identified front are also noted.

Other areas are also identified as possible frontal boundaries in the profiler data. One such region, located near 10 km at 0000 UTC on 18 October, agrees well with the location of a strong stable layer in the sounding data (Fig. 4b) and a local maximum in the SNR (not shown). The stable layer is also present (although not as strong) in the previous sounding (Fig. 4a). The SNR maximum is joined to the descending area at 8 km at 0200 UTC on 18 October, which is also indicated as a front. It is unclear what this boundary represents, and there are no other data available to further investigate the matter. However, given the sounding data and SNR enhancement, this is believed to reflect a real phenomenon, rather than a spurious identification based on random errors (see section 5). One interpretation of these observations is that this is a rapidly descending tropopause, although it is difficult to verify with the available observations. The frontal boundary weakly indicated below 4 km between 0400 and 1100 UTC on 17 October is possibly related to the prefrontal trough noted in Fig. 2a, though this interpretation is also uncertain. To date, there have been relatively few investigations of the Australian prefrontal trough and none have examined the vertical structure of the feature. Other areas, such as region around 7 km throughout 17 October, contain gradients in excess of 3 K (100 km)$^{-1}$, but are not considered fronts as they lack spatial and temporal continuity.

Figure 9b shows contours of the frontal scores for 1200 UTC 18 October to 0000 UTC 20 October. The front is nearly horizontal between 6 and 7 km early in the period. Again, this is mainly a reflection of a strong temperature gradient. This nearly horizontal portion of the front agrees well with the estimated position of the tropopause (vertical bars in Fig. 9b and Fig. 4c). Stable layers in the sounding data are also noted above the height of the profiler-identified front; these result from the relatively stable stratospheric air above the lowered tropopause. A strongly indicated front resumes early on 19 October between 7 and 8 km. Around 0900 UTC, this front ''splits'' into ascending and descending branches that coincide with the onset of the strong S and SW winds (Figs. 7, 8) and the passage of the upper trough (Fig. 3c). The upper branch extends upward to 12 km, while the lower branch reaches down to nearly 2 km toward the end of the period. Extrapolating the position of the lower branch of the front to 0000 UTC gives a reasonable agreement with the sharp inversion noted in the sounding data (Fig. 4d). The height of this

Unauthenticated | Downloaded 10/19/21 07:43 PM UTC

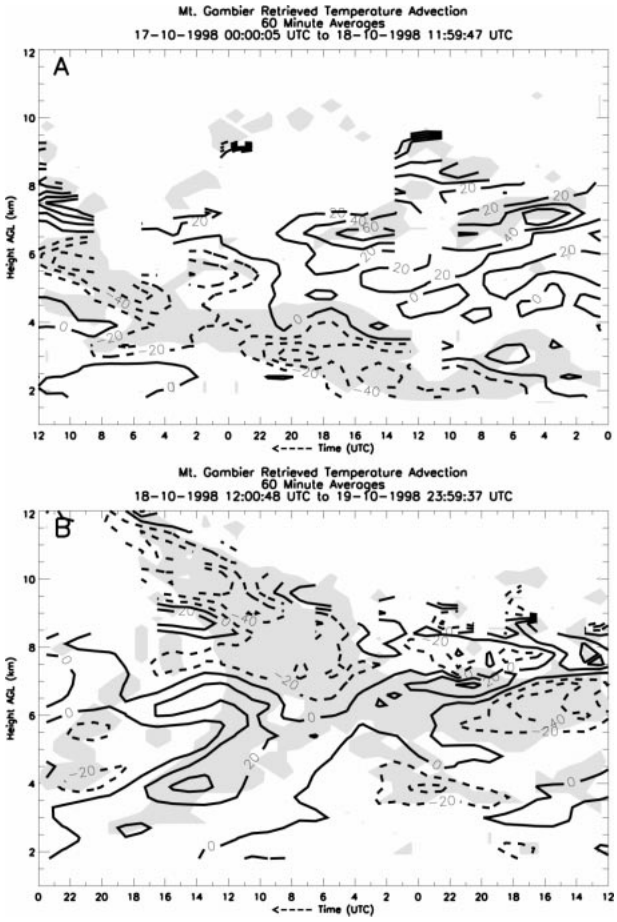

FIG. 10. As in Fig. 4 except for retrieved horizontal thermal advection (K day^{-1}) for (a) 0000 UTC 17 Oct to 1200 UTC 18 Oct 1998 and (b) 1200 UTC 18 Oct to 0000 UTC 20 Oct 1998. Contour interval is 20 K day^{-1}. Negative (cold advection) contours are dashed. Shaded areas depict a frontal score of greater than 1. Three point smoothing in time is applied to advection to reduce noise.

inversion in the sounding is at the lower edge of the available profiler data, where the algorithm has difficulty detecting the fronts as no horizontal temperature gradient is retrieved.

The advection patterns for the two periods are shown in Figs. 10a and 10b. A three-point smoothing in time has been applied to the advection values to reduce the noise in the plots. Frontal scores >1 are shaded to highlight the locations of the fronts identified by the algorithm. Warm advection of about 20–40 K day^{-1}, with peaks exceeding 60 K day^{-1}, is noted throughout the troposphere during the first half of 17 October. Cold advection of over 60 K day^{-1} is suggested with the passage of the main front, indicating that it is a cold front. In the second period, strong cold advection is again noted in the continuation of the main front near 7 km. After the front splits, cold advection exceeding 60 K day^{-1} is noted in the upper branch, suggesting that it is the signature of the rising tropopause or an upper extension of the low-level cold front. In the lower branch, warm advection with a typical magnitude >40 K day^{-1} is seen, suggesting that this is a different (but related) entity. This feature, termed here the trailing front, represents the passage of the upper-level trough over the profiler site. The core of the jet stream moves overhead and warm advection occurs as the cold air in the trough is replaced by warm air in the accompanying ridge, analogous to the situation presented in Neiman and Shapiro (1989) and Neiman et al. (1992) for the continental United States.

Overall, the profiler data and the front-finding algorithm depict a cross section through a classic midlatitude baroclinic wave (e.g., Newton 1958; Palmén and Newton 1969, 183–184). As the cold front arrives at low levels, a strong jet stream with a poleward (northerly, in this case) component is observed in midlevels. As the mid- and upper-level trough moves overhead, the tropopause reaches its lowest height, down to ~6 km in this study. With the passage of the trough, the tropopause ascends to its normal height and a second jet stream with a equatorward component is observed. Associated with this second jet stream is the ''jet front'' or trailing front, where the cold air of the trough is replaced with warmer air. The onset of this second jet stream occurs rapidly. The front-finding algorithm clearly picks out the main cold front, the ascending tropopause and the trailing front (Fig. 9). There are also hints of the descending tropopause and the prefrontal trough, although the data are sparse and inconclusive. The scenario is also generally supported by the routine radiosonde data (Fig. 4), although the location of the tropopause is indistinct during the passage of the trough. Surface and constant pressure charts (Figs. 1 and 3) and vertical cross sections (not shown) from the BoM LAPS forecast model analyses also support this view. However, it must be noted that the depicted fronts do not represent a cross section through a static system. The meteorological situation depicted in this study is evolving, as the trough at 500 hPa clearly strengthens as it moves toward the east. There are also uncertainties involving the time to space conversion of the data. If the system is moving at a constant speed, then the conversion is straightforward. However, if the system is moving at a nonconstant speed or is stationary, these considerations must be taken into account when interpreting the data. This information is not available with the profiler data; other data sources must be utilized to make this determination.

5. Discussion

The example provided demonstrates the ability of the algorithm to identify the fronts associated with a midlatitude baroclinic wave. The algorithm works objectively using only data from the profiler, although the final interpretation is subjective. While it identifies the main frontal features with ease, other regions are also defined as fronts. It is unclear whether these regions

Unauthenticated | Downloaded 10/19/21 07:43 PM UTC

represent some real meteorological phenomena (e.g., gravity waves) or are simply errors in the data and/or analysis. This subject remains under investigation. In this section, errors in the assumptions of the analysis and the data and their potential effects on the analysis are discussed. A few comments about the performance of the algorithm are also provided.

a. Analysis errors

Errors in the frontal analysis would be quite large if the profiler is incorrectly estimating the speed and direction of the wind. To verify that this is not the case and to estimate the magnitude of the errors in the profiler wind measurement, Fig. 11 shows a comparison of the horizontal wind speed and direction from the profiler and the wind flights launched from Mount Gambier for the three days of this study. Eleven wind flights ascents are included, three on 17 October and four each on 18 and 19 October. Hourly averaged wind profiles from the hour nearest the sonde launch time are compared. For the purpose of this comparison, the balloon wind measurements are assumed to represent the true wind. In reality, balloon measurements are subject to an rms uncertainty on the order of 2–3 m s^{-1}. Comparison of the wind speeds (Fig. 11a) shows a distinct bias in the comparison. Wind speeds measured by the profiler are lower than those estimated by the balloon. The magnitude of this bias shows an apparent increase as the wind speed increases. The rms difference in speed between the two estimates is 8.0 m s^{-1}. Examination of the individual wind components (not shown) shows that much of this difference is in the zonal wind. The wind directions (Fig. 11b) in the two measurements are relatively close. The rms difference between the two is just over 6°, with little apparent bias.

Vincent et al. (1998) summarized comparisons of horizontal winds from profilers and other sources that have been reported in the literature. They showed that reported rms differences between profilers and other wind measurements (i.e., balloon, aircraft) range from 1 to 4 m s^{-1}. The large rms differences shown in this study are likely a result of the synoptic situation, as long-term comparisons of balloon and profiler winds at Mount Gambier have a lower uncertainty than those shown here (F. Zink 1999, personal communication). The strong winds observed result in a large displacement of the sonde from its launch point. This leads to the sonde and the profiler sampling different regions of the atmosphere and the natural variability of the wind field may play a role in unduly influencing the comparison. This could be particularly important in the vicinity of a frontal zone, where large variability in the wind fields is often observed. However, this would lead primarily to enhanced scatter in the comparison, rather than a bias. The bias in the profiler wind speed likely reflects shortcomings in the analysis technique used to calculate the winds. Vincent et al. (1987) previously noted a similar bias in tropospheric winds calculated using the spaced-antenna method. As seen here, this bias was noted to increase as the wind speed increases.

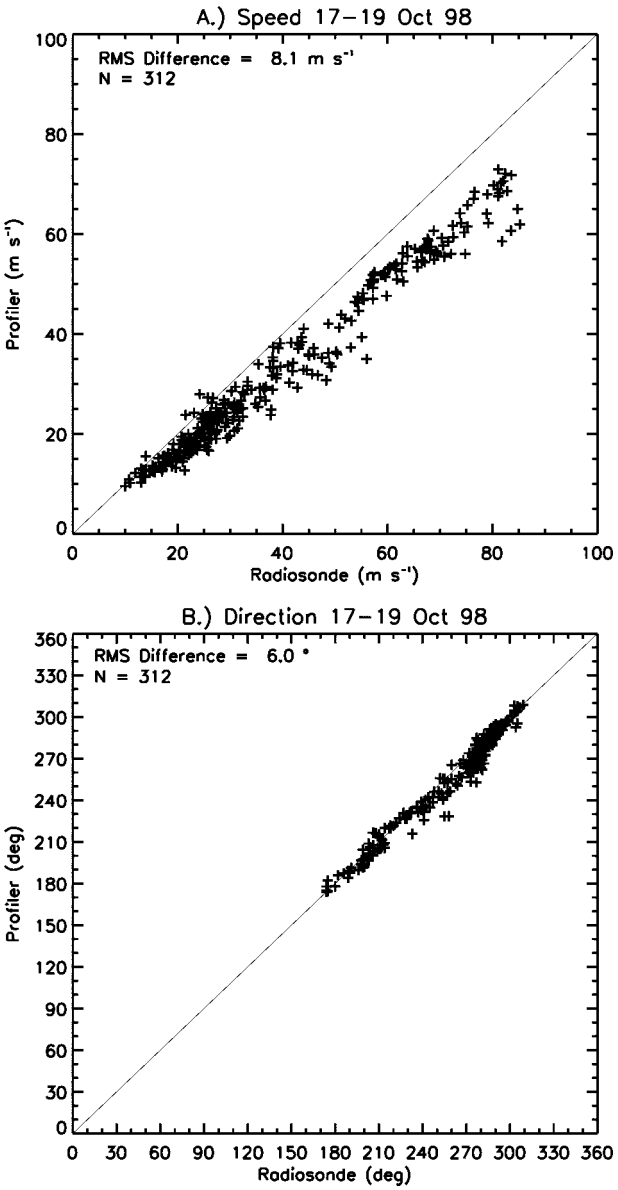

FIG. 11. Comparison of (a) wind speed and (b) wind direction of horizontal winds from radiosonde flights and wind profiler. Hourly averaged profiler winds and 11 radiosonde flights from 17 to 19 October 1998 are used in the comparison. Diagonal line is the one-to-one line and represents a perfect comparison.

A closer examination of the results shows that much of the error is associated with the latter half of 17 October, a period when the jet stream is very strong, the sonde displacement is large, and a strong cold front is in the vicinity of the profiler. Thus, the 1–4 m s^{-1} wind errors reported above are more likely to represent the typical magnitude of error

Errors in the frontal analysis largely arise during the

Unauthenticated | Downloaded 10/19/21 07:43 PM UTC

retrieval of the horizontal temperature gradient. Neiman and Shapiro (1989) examined potential sources of error in this calculation due to the synoptic situation. They found that it is accurate to the degree that the wind is in geostrophic balance. This assumption can be particularly questionable near frontal circulations and in the cyclonically curved flow associated with a trough. These factors potentially result in an underestimation of the true horizontal temperature gradient strength. The direction of the retrieved horizontal temperature gradient is potentially in error when the wind direction and/or the curvature of the flow varies with height. Cross-contour flow results in errors in the direction and magnitude of the retrieved horizontal temperature gradient. For typical short-wave troughs, the magnitudes of the curvature, vertically varying direction and curvature, and cross-contour flow terms are usually less than one-half the magnitude of the purely geostrophic horizontal temperature gradient assumed here. As long as the magnitude of the retrieved horizontal temperature gradient is not reduced below the threshold required to score points, the frontal algorithm will be unaffected. Points will still be accumulated. Errors in the direction of the retrieved horizontal temperature gradient will affect the advection calculation. If the retrieved direction is within 90° of the actual direction the sign of the advection will be correct and the type (i.e., cold or warm) of front can be correctly identified.

The horizontal temperature gradient and advection calculations are also sensitive to errors in the specification of the pressure at the vertical levels, errors in the wind measurement, and the vertical resolution of the data. The sensitivity of these calculations to these sources of error are shown in Table 2. Inaccuracies in gradient and advection calculations discussed here are estimated by selectively introducing random errors of known magnitude into an idealized wind profile with a layer of constant shear. This layer of constant shear corresponds to a retrieved gradient of about 4.5 K (100 km)$^{-1}$ and an advection of around -55 K day^{-1}. The effect of these random errors is estimated 50 times for each error type and magnitude. The rms error estimates on the retrieved horizontal temperature gradient and advection calculations are averaged for the 50 trials. Results are then compared against the known values from the idealized profile to compute the rms difference shown in the table.

In this study, pressure at a given height is assumed to be the average pressure from 17 months (Jan 1998–May 1999) of three or four times daily upper-air wind flights at that level. The standard deviations of pressure in those averages range from 5.5 to 7.5 hPa at heights below 12 km. Errors are imposed with a magnitude of 0.5, 1.0, 1.5, or 2.0 standard deviations. Errors in the gradient and advection calculations with normally distributed uncertainties in pressure are less than ~1 K (100 km)$^{-1}$ and 15 K day^{-1} when their magnitude is 1.5 standard deviations or less, rapidly becoming much larger as the size of the uncertainty is increased. For the more meteorologically realistic case where the errors are all biased in the same direction (but still by a random amount), the errors in the gradient and advection calculations remain less than ~1 K (100 km)$^{-1}$ and 10 K day^{-1} even as the imposed uncertainty grows large.

TABLE 2. Estimates of error on retrieved gradient and advection calculations. Uncertainty is specified to the selected field (type of error) as either a normally or uniformly (biased) distributed random number with a scale given by the imposed rms uncertainty. Gradient and advection errors (last two columns) are reported as an rms difference from an idealized wind profile with a layer of constant shear corresponding to a gradient of 4.5 K (100 km)$^{-1}$ and an advection of -55 K day^{-1}. The numbers in each entry in the table are the average of 50 randomized profiles.

Type of error	Resolution (m)	Imposed rms uncertainty (m s^{-1} or hPa)	Grad. rms error [K (100 km)$^{-1}$]	Adv. rms error (K day^{-1})
Pressure (normal)	300	3.1	0.5	6.6
	300	6.6	0.8	9.3
	300	9.5	1.1	13.0
	300	13.5	4.0	49.5
Pressure (biased)	300	3.6	0.5	6.2
	300	7.2	0.5	6.7
	300	10.9	0.6	7.6
	300	14.8	0.7	8.5
Wind (normal)	300	1.0	0.9	11.0
	300	2.0	1.6	19.8
	300	3.0	2.3	29.3
	300	4.0	3.0	38.7
Resolution (wind only)	100	2.0	4.5	56.5
	200	2.0	2.2	27.4
	300	2.0	1.6	19.8
	600	2.0	1.0	13.4

Estimating the effect of wind errors on the retrieved gradient and advection calculations depends on the type of error specified. Realistic values of normally distributed random uncertainties in the wind produce larger errors in the retrieved gradient and advection than those associated with the specification of the pressure. Table 2 shows that the magnitude of the error increases with the uncertainty. For random rms wind errors of less than 3 m s^{-1}, the uncertainty in the computed gradients is below 2.5 K (100 km)$^{-1}$. These values stay approximately the same regardless of the value of gradient strength imposed. This is not the case with the advection calculation, which is the product of the retrieved gradient and the wind speed. While generally increasing as errors in the wind increase, advection errors are less at lower wind speed and more at higher wind speeds. Similarly, adding a constant bias (not shown) results only in errors to the advection field. The vertical shear, which determines the gradient strength, remains the same while the bias alters the wind speed and thus the advection calculation. The gradient and advection calculations are also very sensitive to the vertical resolution of the profiler data. With high resolution, even small errors in the wind measurement are magnified. However, little im-

Unauthenticated | Downloaded 10/19/21 07:43 PM UTC

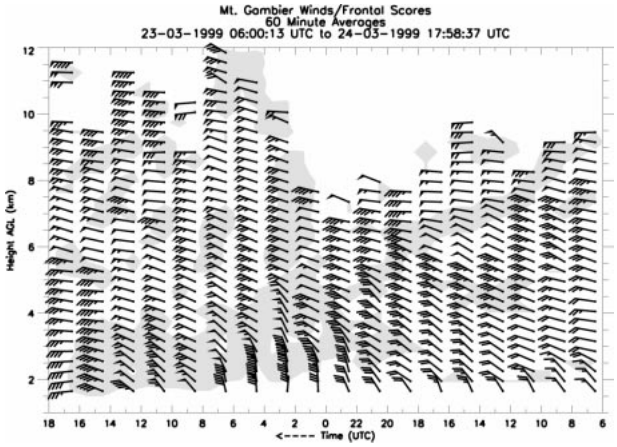

FIG. 12. Time–height cross section of hourly averaged horizontal wind from the Mount Gambier VHF profiler for 0600 UTC 23 Mar to 1800 UTC 24 Mar 1999. Barbs as in Fig. 3. Winds plotted every 2 h for clarity. Frontal scores >1 are shaded.

provement is seen by lowering the resolution below the 300 m used in this study.

The largest source of error in this algorithm lies with the uncertainty in the wind measurements. In this study, as in Vincent et al. (1987), the winds measured by the radar using the spaced-antenna method are weaker than those measured by balloon, particularly when a strong jet stream is observed. Superposed over this apparent bias are smaller, random errors. The bias has relatively little effect, creating a small bias in the calculated advection, while the random errors create uncertainties in the horizontal temperature gradient on the order of 1.5–2.5 K (100 km)$^{-1}$. For a $\sim$20 m s^{-1} wind, the value in Table 2, errors in the thermal advection are on the order of 20–30 K day^{-1}. These error estimates assume that the wind is geostrophic. Deviations from geostrophy would further increase the error. Errors due to the specification of pressure are relatively small in this case, as the pressures from the radiosondes are within one to two standard deviations of the average pressure specified. Errors from this source would be larger in the case of an extreme deviation from the mean profile. Overall, these estimates suggest that much of the ''noise'' in the frontal analysis is due to errors in the data rather than actual meteorological phenomena, but that possibility cannot be discounted.

b. Algorithm performance

In this section, the general performance of the algorithm is discussed. The frontal system provided as an example in section 4 is quite strong and readily identifiable. In many situations, the fronts are not as strongly defined. One such example is shown in Fig. 12. This figure, showing the hourly winds and frontal scores >1 for 23–24 March 1999, depicts a warm front associated with the remnants of Tropical Cyclone Vance, a category 5 tropical cyclone that passed over WA, turned extratropical, and subsequently moved to the south of the profiler site. The warm front extends downward from near 9.5 km at 0600 UTC on 23 March to near 2 km beginning around 0800 UTC on 24 March. In the upper portion of the warm front, the frontal scores are quite low, but continuity in time and space is distinctly visible. Frontal scores are higher at lower altitudes. These scores are associated with a weak thermal gradient [2–3 K (100 km)$^{-1}$] with warm advection. The front is also accompanied by a subtle shift in the winds from N and NW ahead to more westerly winds behind. An examination of the sounding data during this period (not shown) shows a distinct discontinuity in relative humidity corresponding with the location of the frontal boundary. Above the discontinuity, the relative humidity is quite high, with values ranging from 70% to near saturation. Below the front, the air is rather dry, with relative humidity values at 40% and below. The heights of this discontinuity in the sounding data compare very well with the region identified as the frontal zone by the algorithm. Stronger upward motion is also apparent behind the warm front (not shown). This is a subtle feature, particularly the upper portion, which would likely be overlooked without the application of the algorithm. As discussed above, other regions are also spuriously identified as frontal zones, both ahead of and behind the warm front. The regions between 6 and 9 km centered at 0300 UTC on 24 March is associated with a strong jump in the SNR, also shown by the increase in reliable data at that time.

To date, the algorithm has been run on about 2 yr of data from the Mount Gambier profiler site. Numerous frontal systems have been observed during that time. In general, whenever a cold front is indicated on the surface chart, a corresponding feature can be identified in the profiler data using the algorithm. Some of these fronts are only loosely defined by the algorithm, although these tend to correspond with weaker fronts with little thermal contrast. Warm fronts are not routinely analyzed by the BoM and thus cannot be verified in a straightforward manner. Trailing fronts, as discussed in section 4 of this paper, are also indicated in many cases, and these correspond to the passage of the upwind side of a baroclinic wave over the profiler. Weak baroclinic troughs are also often detected, appearing similarly to the trailing front but unassociated with other fronts. In general, when no fronts or baroclinic waves are indicated in the analyses, then nothing is indicated by the algorithm. One exception is a persistent stable layer associated with subsidence inversions from the subtropical ridge, which can be weakly detected as a nearly ''horizontal'' front. More detail of these features will be described in a future paper.

Overall, the algorithm performs well in a variety of meteorological situations. However, it should be noted that the results discussed here have been obtained using profilers operating at VHF (50 MHz). These frequencies

Unauthenticated | Downloaded 10/19/21 07:43 PM UTC

are relatively insensitive to Rayleigh scattering from precipitation. The SNR is not dramatically increased by, and the radar can still easily measure winds in, precipitation. This is not always the case for profilers operating at higher frequencies (e.g., 449 or 915 MHz), where measurement of clear-air properties in precipitation is more problematic and Rayleigh scaterring from precipitation is more dominant. This is a potential limitation for the application of the algorithm at higher frequencies. To overcome this limitation, the SNR criterion could be omitted with the loss of some ability to reliably detect upper fronts. Where reliable estimates of the wind are available in precipitation (Wuertz et al. 1988), the algorithm could still be run with some success.

6. Conclusions

In this study, an algorithm to identify frontal zones in wind profiler data is described. The algorithm objectively identifies possible frontal zones. A subjective examination of the results is needed to separate actual frontal zones and noise. A study of a strong springtime frontal system over South Australia is presented from the perspectives of a traditional synoptic analysis and the profiler data. The two analyses agree well in their identification of the fronts. A discussion of the potential errors is also presented.

The algorithm works by identifying regions with 1) a strong horizontal temperature gradient, estimated using the quasigeostrophic thermal wind retrieval technique given by Neiman and Shapiro (1989); 2) a temporal increase in the signal-to-noise ratio at a given range gate; and/or 3) a strong temporal shift in the horizontal winds at a given range gate. These criteria utilize the basic definition of a front and the methodologies employed by other researchers, which have been used to identify fronts in profiler data. The type of front can be determined by examining the associated advection field and the characteristics of the boundary.

The cold front in the example shown here is identified mainly by the strong horizontal temperature gradient. A slight wind shift is also seen. The SNR portion of the algorithm is only of minor importance in this case, picking up hints of a descending tropopause. Other cases examined show that this aspect of the algorithm is useful for detecting warm fronts and the shallow summertime cool changes seen over South Australia (e.g., Wilson and Stern 1985).

Comparison of radiosonde and profiler winds suggests that the profiler is underestimating wind speed during this period. This is the result of the known bias in the spaced-antenna technique used to estimate the wind speed (Vincent et al. 1987) and the strong jet stream present, which results in the radiosonde and profiler sampling different regions of the atmosphere, thus potentially increasing the scatter of the comparison. These errors potentially have an adverse effect on the analysis and likely account for some of the noise seen in the frontal analysis, although meteorological features with a short timescale cannot be ruled out. The wind bias could also result in an underestimate of the advection associated with the front. Smaller, random errors could also have a detrimental effect on the gradient and advection calculations.

The algorithm is simple, quick, and easily applied to profiler data from any location. Different types of frontal zones can be reliably detected. It can be run in real time to aid in the diagnosis and forecasting of frontal systems, as well as during postprocessing for research purposes such as the verification of high-resolution operational forecast models and the verification of composite studies of fronts in southern Australia. The scheme can also be easily adapted for use with output from operational forecast models such as LAPS and MESO-LAPS, its higher resolution (0.125°) counterpart. In a future paper, we will use this algorithm to construct a census of frontal systems over South Australia, documenting their physical characteristics throughout the year. Verification studies as mentioned above will also be performed.

Acknowledgments. This research is supported by Australian Research Council Grant A69802414. Graham Mills, John Bally, and two anonymous reviewers are thanked for their constructive comments on the manuscript. Surface data were provided by the BoM Regional Forecast Office in Adelaide.

REFERENCES

Briggs, B. H., 1984: The analysis of spaced sensor records by correlation techniques. *Handbook for the Middle Atmosphere Program,* R. A. Vincent, Ed., Vol. 13, SCOSTEP Secrt., Univ. of Illinois, Urbana, IL, 166–186.

Browning, K. A., D. Jerrett, J. Nash, T. Oakley, and N. M. Roberts, 1998: Cold frontal structure derived from radar wind profilers. *Meteor. Appl.,* **5,** 67–174.

Caccia, J.-L., and J.-P. Cammas, 1998: VHF–ST radar observations of an upper-level front using vertical and oblique-beam C_N^2 measurements. *Mon. Wea. Rev.,* **126,** 483–501.

Crochet, M., F. Cuq, F. M. Ralph, and S. V. Venkateswaren, 1990: Clear-air radar observations of the great October storm of 1987. *Dyn. Atmos. Oceans,* **14,** 443–461.

Griffiths, M., M. J. Reeder, D. J. Low, and R. A. Vincent, 1998: Observations of a cut-off low over southern Australia. *Quart. J. Roy. Meteor. Soc.,* **124,** 1109–1132.

Hanstrum, B. N., K. J. Wilson, and S. L. Barrell, 1990: Pre-frontal troughs over southern Australia. *Wea. Forecasting,* **5,** 22–31.

Keyser, D., and M. A. Shapiro, 1986: A review of the structure and dynamics of upper-level frontal zones. *Mon. Wea. Rev.,* **114,** 452–499.

Larsen, M. F., and J. Röttger, 1982: VHF and UHF Doppler radars as tools for synoptic research. *Bull. Amer. Meteor. Soc.,* **63,** 996–1008.

——, and ——, 1983: Comparison of tropopause height and frontal boundary locations based on radar and radiosonde data. *Geophys. Res. Lett.,* **10,** 325–328.

——, and ——, 1985: Observations of frontal zone and tropopause structures with a VHF Doppler radar and radiosondes. *Radio Sci.,* **20,** 1223–1232.

May, P. T., K. J. Wilson, and B. F. Ryan, 1990: VHF radar studies of cold fronts traversing southern Australia. *Beitr. Phys. Atmos.,* **63,** 257–269.

Unauthenticated | Downloaded 10/19/21 07:43 PM UTC

——, M. Yamamoto, S. Fukao, T. Sato, S. Kato, and T. Tsuda, 1991: Wind and reflectivity fields around fronts observed with a VHF radar. *Radio Sci.,* **26,** 1245–1249.

Neiman, P. J., and M. A. Shapiro, 1989: Retrieving horizontal temperature gradients and advections from single-station wind-profiler observations. *Wea. Forecasting,* **4,** 222–233.

——, P. T. May, and M. A. Shapiro, 1992: Radio Acoustic Sounding System (RASS) and wind profiler observations of lower- and mid-tropospheric weather systems. *Mon. Wea. Rev.,* **120,** 2298–2313.

Newton, C. W., 1958: Variations in frontal structure of upper-level troughs. *Geophysica,* **6,** 357–375.

Palmén, E., and C. W. Newton, 1969: *Atmospheric Circulation Systems.* Academic Press, 603 pp.

Puri, K., G. S. Dietachmayer, G. A. Mills, N. E. Davidson, R. A. Bowen, and L. W. Logan, 1998: The new BMRC Limited Area Prediction System, LAPS. *Aust. Meteor. Mag.,* **47,** 203–223.

Reid, I. M., B. H. Johnson, D. A. Holdsworth, A. D. MacKinnon, J. Strickland, R. A. Vincent, and F. Zink, 1998: A new VHF radar for use in operational meteorology. *Extended Abstracts, Fourth Int. Symp. on Tropospheric Profiling: Needs and Technologies,* Snowmass, CO, University of Colorado, 264–266.

Shapiro, M. A., and D. Keyser, 1990: Fronts, jet streams and the tropopause. *Extratropical Cyclones: The Erik Palmén Memorial Volume,* C. W. Newton and E. O. Holopainen, Eds., Amer. Meteor. Soc., 167–191.

——, T. Hampel, D. Rotzoll, and F. Mosher, 1985: The frontal hydraulic head: A microscale (1 km) triggering mechanism for mesoconvective weather systems. *Mon. Wea. Rev.,* **113,** 1166–1183.

Tsuda, T., P. T. May, T. Sato, S. Kato, and S. Fukao, 1988: Simultaneous observations of reflection echoes and refractive index gradient in the troposphere and lower stratosphere. *Radio Sci.,* **23,** 655–665.

Vincent, R. A., P. T. May, W. K. Hocking, W. G. Elford, B. H. Candy, and B. H. Briggs, 1987: First results with the Adelaide VHF radar: Spaced antenna studies of tropospheric winds. *J. Atmos. Terr. Phys.,* **49,** 353–366.

——, S. Dullaway, A. MacKinnon, I. M. Reid, F. Zink, P. T. May, and B. H. Johnson, 1998: A VHF boundary layer radar: First results. *Radio Sci.,* **33,** 845–860.

Wilson, K. J., and H. Stern, 1985: The Australian summertime cool change. Part I. Synoptic and subsynoptic aspects. *Mon. Wea. Rev.,* **113,** 177–201.

WMO, 1957: Definition of the tropopause. *WMO Bull.,* **6,** 136.

Wuertz, D. A., B. Weber, R. G. Strauch, A. S. Frisch, G. Little, D. A. Merritt, K. P. Moran, and D. C. Welsh, 1988: Effects of precipitation on UHF wind profiler measurements. *J. Atmos. Oceanic Technol.,* **5,** 450–465.

Unauthenticated | Downloaded 10/19/21 07:43 PM UTC